Technetium incorporation into goethite (α-FeOOH): An atomic-scale investigation

Frances N. Smith[†], Christopher D. Taylor[§], Wooyong Um[†], and Albert A. Kruger[††]*

[†]Pacific Northwest National Laboratory, 902 Battelle Boulevard, Richland, WA, 99354

[§] Fontana Corrosion Center, Materials Science and Engineering, The Ohio State University, Columbus OH 43210; Strategic Research and Innovation, DNV GL, Dublin OH 43017

[††] United States Department of Energy, Office of River Protection, P.O. Box 450, Richland, WA 99352

*Corresponding Author contact information: Address: Pacific Northwest National Laboratory, P.O. Box 999, MS-IN P7-25, Richland, WA, 99352. E-mail: frances.smith@pnnl.gov. Phone: 509-375-5645. Fax: 509-375-5684.

Summary of Supporting Information:

14 pages (including cover page), 3 figures and 4 tables

Computational Details

Table S1. Results from Basis Set Testing of Representative Oxides for Fe(II), Fe(III), and Tc(IV) with Lowest Energy Magnetic Structure Ordering

Phase	Total Energy (eV)	Lattice Param. a (Å)	Lattice Param. b (Å)	Lattice Param. c (Å)	Alpha (degrees)	Beta (degrees)	Gamma (degrees)	Volume (Å^3)
FeO (AFM-111)	-32360.36	8.800	8.803	8.784	89.927	89.809	89.884	680.475
*Experimental**		8.652	8.652	8.652	90.000	90.000	90.000	647.664
Difference (%)		*1.713*	*1.747*	*1.524*	*-0.081*	*-0.212*	*-0.128*	*5.066*
Fe_2O_3 (AFM)	-541.0205	5.119	5.119	13.735	90.000	90.001	119.999	311.734
Experimental†		5.038	5.038	13.772	90.000	90.000	120.000	302.722
Difference (%)		*1.615*	*1.611*	*-0.267*	*0.000*	*0.001*	*-0.001*	*2.977*
TcO_2 (AFM)	-172.6415	6.227	4.526	5.505	90.000	124.493	89.999	127.895
Experimental‡		5.689	4.755	5.520	90.000	121.453	90.000	127.362
Difference (%)		*9.457*	*-4.799*	*-0.258*	*0.000*	*2.502*	*-0.001*	*0.418*

*Fjellvåg et al.[1]

†Blake et al.[2]

‡Rodriguez et al.[3]

Effective core potential (ECP) basis sets were used to describe all the elements used in this study. For O and Fe, Durand ECPs were used such that core orbitals for [He] were captured by the ECP, and valence orbitals $2s^2 2p^6$ were expressed explicitly for O^{2-}. For Fe, core orbitals for [Ar] were captured by the ECP and valence orbitals $4s^0 3d^6$ and $4s^0 3d^5$ were expressed for Fe^{2+} and Fe^{3+}, respectively.[4] For Tc^{4+}, the Hay and Wadt large core ECP (HAYWLC) was used that captures [Kr] core orbitals and expresses $5s^0 4d^3$ valence orbitals explicitly.[5]

For wüstite (FeO), a structure was generated using crystallographic data from Fjellvåg et al.[1] Comparisons were made between one ferromagnetic (all Fe(III) spin up) model with space group symmetry (225; net spin 128), and two anti-ferromagnetic spin orderings with *P1* symmetry where every iron layers alternated between Fe(III) spin up and Fe(III) spin down along the <111> versus <100> crystallographic directions. Here, the "FeII" basis set describing

octahedrally coordinated iron from Iordanova et al.[4] is used with an electron occupancy of 6 instead of 5 in the *3d* orbital level. A Durand-41G ECP Crystal basis set for oxygen is used in conjunction.[4, 6]

For hematite (α-Fe_2O_3), a structure was generated using crystallographic information from Blake et al.[2] Comparisons were made between three atomic-scale models: 1) ferromagnetic with space group symmetry (167; net spin 5); 2) ferromagnetic with P1 symmetry (net spin 60); and, 3) anti-ferromagnetic with P1 symmetry where every other (001) iron bi-layer is spin up or spin down. The effective-core potential (ECP) "FeII" basis set from Iordanova et al.[4] was used which was optimized to described octahedrally coordinated iron atoms. A Durand-41G ECP Crystal basis set for oxygen is used in conjunction.[4, 6]

For technetium dioxide (TcO_2), a structure was generated using crystallographic data from Rodriguez et al.[3] Comparisons were made between three atomic-scale models: 1) ferromagnetic with space group symmetry (14; net spin 3); 2) ferromagnetic with P1 symmetry (net spin 12); and 3) anti-ferromagnetic with P1 symmetry (net spin 0) with every other Tc atom is assigned spin-up or spin-down behavior parallel to the y-axis of the crystal. The Tc^{4+} basis set from Skomurski et al.[5] is used which was optimized to describe octahedrally-coordinated Tc^{4+}. A Durand-41G ECP Crystal basis set for oxygen is used in conjunction.[4, 6]

Table S2. Total Energy versus k-point Density in a Single, Ferromagnetic (FM) Goethite Unit Cell

# k-points	Single-Point Energy (Ha)	Energy Difference (n-(n-1)) (Ha)	Energy Difference (n-(n-1)) (eV)
1	-772.70401	----	----
8	-214.09426	558.60975	15200.32991
14	-214.11287	-0.01861	-0.50640
36	-214.11397	-0.00110	-0.02993
63	-214.11405	-0.00008	-0.00218
112	-214.11406	-0.00001	-0.00027

Note: Here, "n" refers to the current case, and "n-1" to the previous case.

In **Table S2**, energy differences in column three are reported in Hartrees and converted to electron volts (eV) in column four (1 Ha = 27.211 eV). In these calculations, the atomic positions, lattice parameters, and magnetic ordering of the iron atoms stayed the same while only the k-point density changed. Here, a ferromagnetic (FM) case was used where all iron atoms had the same direction of unpaired spins (e.g., all spin up). A significant change in energy occurs when k-point density increases from 1 k-point in crystallographic space to 8 k-points; this result suggests that the single k-point was not robustly capturing the electronic structure of the goethite unit cell. Based on the minimal change in energy between 63 versus 112 k-points, the former was chosen for all models to maximize computational resources while appropriately capturing the behavior of atoms in the goethite unit cell. A level shift of 10, equal to 1.0 Ha or 27.211 eV, was applied to each calculation to help stabilize charge and spin density.

Magnetic Structure Testing

Regarding the magnetic structure of goethite, experimental studies suggest that it is antiferromagnetic at room temperature[7-9] given the Néel temperature of 130°C.[7] To achieve this, the four iron atoms in the unit cell must have equal and opposite, unpaired spin directions (e.g., 5 unpaired d-orbital electrons per each Fe^{3+}). To determine which magnetic ordering scheme has the lowest optimized energy in goethite, four different cases were tested (see **Figure S1**): (a) ferromagnetic (FM; ++++) where all Fe(III) atoms have the same spin direction; (b) anti-ferromagnetic (AFM; +-+-) where edge-sharing Fe(III) have opposite spin directions to each other, as well as the corner sharing Fe(III) atoms; (c) anti-ferromagnetic-prime (AFM-P; +--+) where edge-sharing Fe(III) have the same spin and opposite spin from the corner sharing Fe^{3+}; and (d) anti-ferromagnetic double-prime (AFM-DP; --++) where edge sharing Fe(III) have opposite spin, but the same spin as neighboring, corner sharing Fe(III). These naming conventions follow those established in Guo and Barnard[10] and Alexandrov and Rosso[11] for ease of comparison, and +/- signs refer to Fe atoms parallel to the *b* axis. The FM case has a net spin of 20 per unit cell; all other AFM cases have a net spin of 0.

To test for the lowest-energy magnetic structure, fixed-cell and full-cell geometry optimizations were performed on each model. Total energy results are shown in **Table S3.** Relative trends indicate that AFM-P(+--+) and AFM (+-+-) cases are nearly equivalent with the lowest energy values, followed by the FM (++++) case, and the AFM-DP (--++) case with the highest optimized, or least favorable, energy values. The two lowest-energy cases differ by only 0.0054 eV, and the two highest-energy cases by only 0.0082 eV; however, differences between the lowest- and highest-energy magnetic structures (AFM-P and AFM-DP, respectively) are an order of magnitude greater in energy (e.g., 0.0680 eV).

When comparing these results to computational studies on geometry-optimized goethite models found in the literature, the AFM and AFM-P magnetic ordering cases have the lowest reported energies, with the AFM structure being approximately 0.027 eV more favorable than the AFM-P structure, according to Guo and Barnard.[10] In that study, the AFM-DP was also the least favorable case, by approximately 0.2721 eV, with ferri- and ferromagnetic cases being somewhere in between. Similar trends were calculated by Alexandrov and Rosso,[11] as well as Fuente et al.,[12] with the AFM case being the lowest in energy of the three different AFM cases tested. Experimental Mössbauer spectroscopy studies also suggest that the AFM structure is also observed at room temperature;[7] however, recent papers outline the complexity in determining the magnetic structure in goethite resulting from some magnetic orderings exhibiting similar energies to one another,[13] as is observed with the two lowest energy cases here. Given the smaller difference in energy between the two lowest-energy cases calculated here (AFM-P and AFM), and in keeping with the majority of theoretical and experimental studies, AFM ordering was used to generate supercells for Tc-incorporation models.

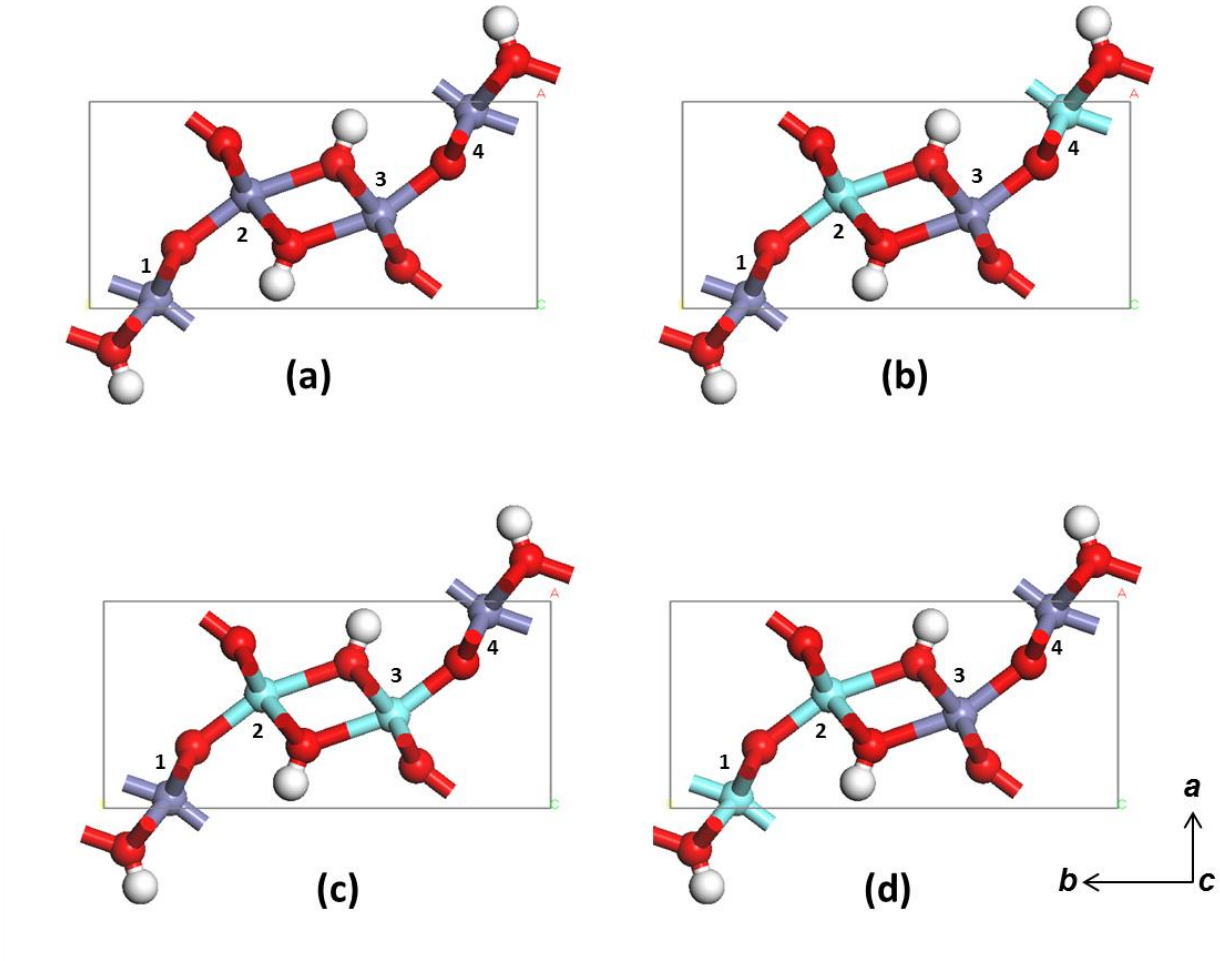

Figure S1. Four different magnetic structures for goethite represented by a single unit cell: a) ferromagnetic (FM; ++++); b) anti-ferromagnetic (AFM; +-+-); c) anti-ferromagnetic prime (AFM-P; +--+); and d) anti-ferromagnetic double-prime (AFM-DP; --++). Purple spheres are Fe(III) (spin up, +), cyan spheres are Fe(III) (spin down, -), red spheres are O^{2-}, and white spheres are H^{+}. Numbers refer to individual iron atoms along the crystallographic *b*-axis.

Table S3. Comparison of Atom-Only versus Full-Lattice Optimized Energy Results for Different Magnetic Ordering Schemes in Single Unit Cells of Goethite

Magnetic Ordering Scheme	Atom-Optimized Energy (eV)	Lattice-Optimized Energy (eV)	a (Å)	b (Å)	c (Å)	α (°)	β (°)	γ (°)	Volume (Å^3)
FM (++++)	-5827.64	-5827.80	4.5404	9.8600	3.1021	89.8665	90.0895	90.3444	138.87
Difference (calc/exp)			*-1.2*	*-0.9*	*2.8*	*-0.1*	*0.1*	*0.4*	*0.6*
AFM (+-+-)	-5827.70	-5827.85	4.5574	9.8688	3.1014	89.8797	90.0933	90.3103	139.49
Difference (calc/exp)			*-0.9*	*-0.8*	*2.8*	*-0.1*	*0.1*	*0.3*	*1.0*
AFM-P (+--+)	-5827.70	-5827.86	4.5551	9.8641	3.1013	89.8770	90.0944	90.3167	139.35
Difference (calc/exp)			*-0.9*	*-0.9*	*2.8*	*-0.1*	*0.1*	*0.4*	*0.9*
AFM-DP (--++)	-5827.63	-5827.79	4.5453	9.8691	3.1030	89.8672	90.0901	90.3395	139.19
Difference (calc/exp)			*-1.1*	*-0.8*	*2.8*	*-0.1*	*0.1*	*0.4*	*0.8*
Experimental[†]	----	----	4.5979	9.9510	3.0178	90.0000	90.0000	90.0000	138.08

[†] Yang et al.[8]; Note: Magnetic ordering schemes correspond to **Figure S1.**

Incorporation Energy Calculations

Table S4. Calculated versus Experimental Ionization Energies

Atom	Electron Config.	Optimized E / atom (Ha)	Optimized E / atom (eV)	Calc. I.E. (eV/atom)	Exper[†] / (eV/atom)	Ionization Step
Fe	$[Ar]4s^2 3d^6$	-20.08	-546.35	----	----	----
Fe^{1+}	$[Ar]4s^1 3d^6$	-20.58	-560.05	-13.70	7.90	First
Fe^{2+}	$[Ar]4s^0 3d^6$	-20.49	-557.57	2.49	16.20	Second
Fe^{3+}	$[Ar]4s^0 3d^5$	-19.49	-530.44	27.13	30.65	Third
Tc	$[Kr]5s^2 4d^5$	-9.76	-265.62	----	----	----
Tc^{1+}	$[Kr]5s^1 4d^5$	-9.95	-270.71	-5.10	7.12	First
Tc^{2+}	$[Kr]5s^0 4d^5$	-10.79	-293.66	-22.95	15.26	Second
Tc^{3+}	$[Kr]5s^0 4d^4$	-9.78	-266.09	27.57	29.55	Third
Tc^{4+}	$[Kr]5s^0 4d^3$	-8.19	-222.74	43.35	41.0	Fourth
O	$[He]2s^2 2p^4$	-15.66	-426.19	----	----	----
O^-	$[He]2s^2 2p^5$	-15.62	-425.04	1.15	1.46*	First
O^{2-}	$[He]2s^2 2p^6$	-15.16	-412.41	12.63	----	Second

*From Neumark et al.[14]

[†]All ionization energies come from NIST[15] unless otherwise noted.

Incorporation Energy Results

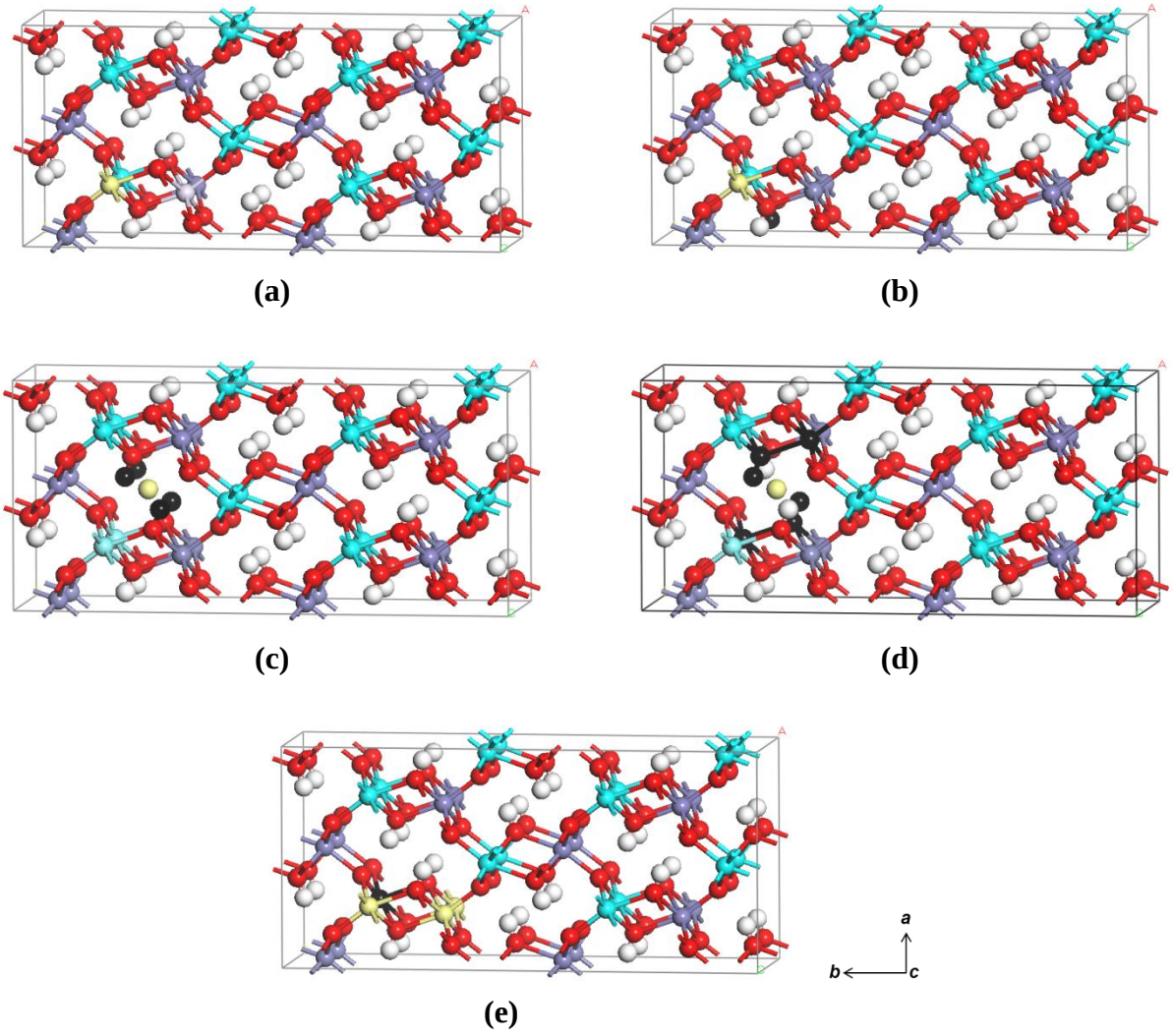

Figure S2. Comparison of five different charge-balanced Tc(IV) incorporation models: (a) Fe(II)-balanced; (b) H^+-vacancy; (c) Tc(IV) interstitial charge-balanced by removal of $4H^+$; (d) Tc(IV) interstitial charge-balanced by removal of two Fe(III)(OH) groups; (e) Fe(III)-vacancy driven. Purple and cyan spheres are Fe(III) spin-up and spin-down, respectfully; red spheres are O^{2-}, white spheres are H^+; yellow spheres are Tc(IV) and light purple sphere is Fe(II). Black spheres indicate atoms that have been removed. The spin of the lattice atoms being replaced dictates the spin of the substituents, except for interstitial atoms which are all spin-up.

Hydrogen Movement

In order to better understand the effects of lattice parameter constraints on hydrogen migration in the goethite system, a comparison was made for the "Fe(III) vacancy" case, where three Tc(IV) are substituted for four lattice Fe(III). In **Figure S3a**, the starting model is overlain by the optimized fixed-cell geometry, where only atom positions were allowed to move. In **Figure S3b**, the same starting model is used, but an optimized model is overlain where both lattice parameters and atomic positions were allowed to move. In **Figure S3a**, two pairs of bridging hydroxyl groups move to bridging oxygen sites directly adjacent to the Fe(III) vacancy, and to bridging oxygen sites adjacent to lattice Fe(III) atoms directly bridged to or in next-nearest neighbor positions to the Fe(III) vacancy.

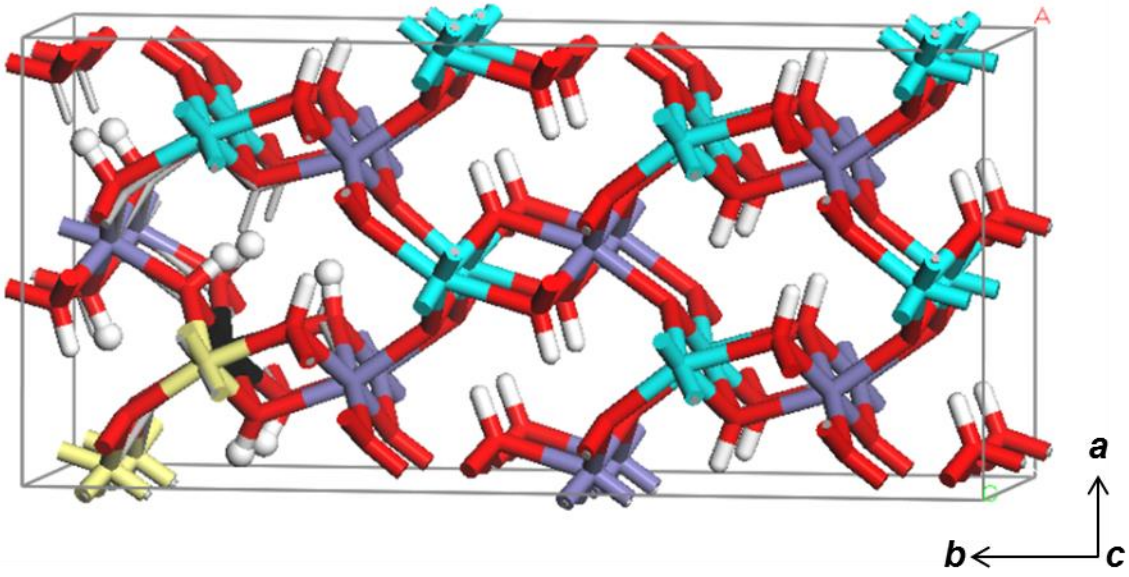

Figure S3a. Fixed-cell "Fe(III)-vacancy" geometry (colored) overlaying starting geometry (gray sticks). Yellow sticks are Tc(IV), purple sticks are Fe(III) spin up, cyan sticks are Fe(III) spin down, red

sticks are O^{2-}, and white sticks are H^{+}. For H^{+} where significant movement occurred relative to the starting model, hydrogen is represented as a white sphere.

For the full-optimized geometry case in **Figure S3b**, only one pair of bridging hydroxyls moves to bridging oxygens associated with the the nearest-neighbor and next-nearest neighbor lattice Fe(III) atoms; however, greater attraction of existing bridging hydroxyl groups towards the Fe(III) defect is observed as a charge-compensating mechanism instead. In both cases, proton movement is observed to help offset electron density deficits created by the Fe(III) vacancy, but in the full optimization case, overall lattice expansion and pointing of existing hydroxyls towards the defect also serve as energy-lowering mechanisms.

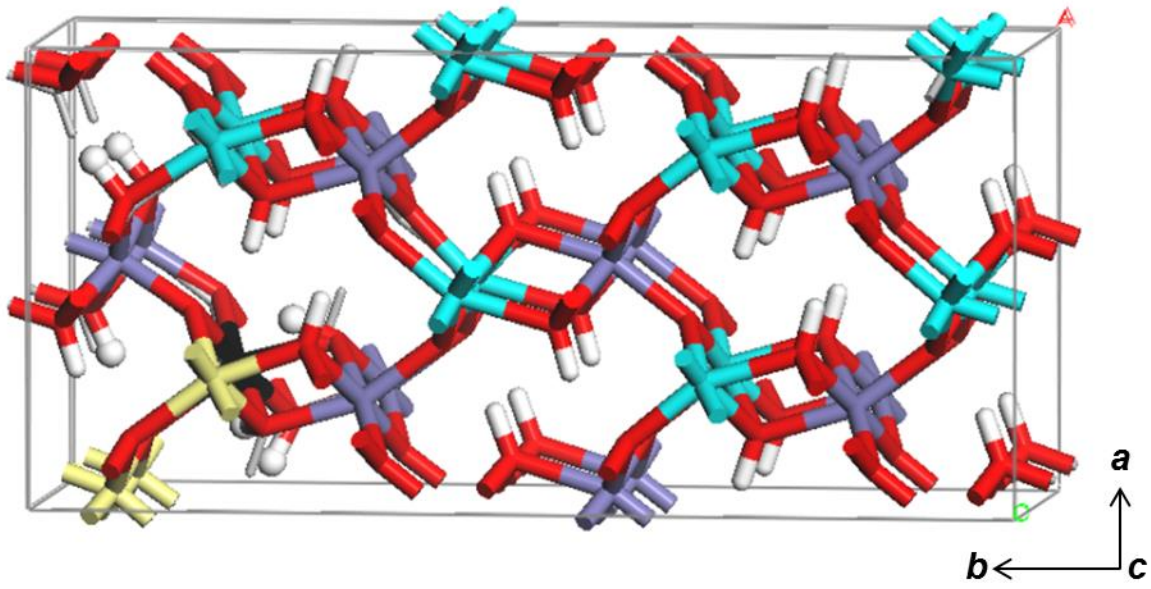

Figure S3b. Fully-relaxed "Fe(III)-vacancy" geometry (colored) overlaying starting geometry (gray sticks). Yellow sticks are Tc(IV), purple sticks are Fe(III) spin up, cyan sticks are Fe(III) spin down, red sticks are O^{2-}, and white sticks are H^{+}. For H^{+} where significant movement occurred relative to the starting model, hydrogen is represented as a white sphere.

An explanation for the movement of hydroxyls associated with the lattice Fe(III) atoms directly bridged to the Fe(III) defect or in the next-nearest neighbor positions may also have to do with proximity to the substituted Tc(IV). Since these are periodic conditions, another supercell would be stacked in all directions surrounding the supercell shown. The bridging oxygens nearest the Tc(IV) defects would be receiving more electron density from Tc(IV) than from Fe(III); as such, movement of protons to bridging oxygen sites associated with Fe(III) instead, as observed for both cases, could also help to lower the energy of the system. In both models, there is contraction of the O-O distances nearest the Fe(III) vacancy compared to the right side of the system which may also facilitate proton movement.

References

1. Fjellvåg, H.; Hauback, B. C.; Vogt, T.; Stølen, S., Monoclinic nearly stoichiometric wüstite at low temperatures. *American Mineralogist* **2002,** *87*, 347-349.
2. Blake, R. L.; Hessevick, R. E.; Zoltai, T.; Finger, L. W., Refinement of the hematite structure. *American Mineralogist* **1966,** *51*, 123-129.
3. Rodriguez, E. E.; Poineau, F.; Llobet, A.; Sattelberger, A. P.; Bhattacharjee, J.; Waghmare, U. V.; Hartmann, T.; Cheetham, A. K., Structural studies of TcO_2 by neutron powder diffraction and first-principles calculations. *Journal of the American Chemical Society* **2007,** *129*, 10244-10248.
4. Iordanova, N.; Dupuis, M.; Rosso, K. M., Charge transport in metal oxides: A theoretical study of hematite a-Fe_2O_3. *J. Chem. Phys.* **2005,** *122*, 144305-1-10.
5. Skomurski, F. N.; Rosso, K. M.; Krupka, K. M.; McGrail, B. P., Technetium incorporation into hematite (a-Fe_2O_3). *Environ. Sci. Technol.* **2010,** *44*, 5855-5861.
6. Apra, E. Ph.D. thesis, University of Torino, 1992.
7. Forsyth, J. B.; Hedley, I. G.; Johnson, C. E., The magnetic structure and hyperfine field of goethite (a-FeOOH). *J. Phys. Chem. C (Proc. Phys. Soc.)* **1968,** *2*, (1), 179-188.
8. Yang, H.; Lu, R.; Downs, R. T.; Costin, G., Goethite, a-FeO(OH), from single-crystal data. *Acta Crystallogr.* **2006,** *E62*, i250-i252.
9. Llavona, Á.; Prados, A.; Velasco, V.; Crespo, P.; Sánchez, M. C.; Pérez, L., Electrochemical synthesis and magnetic properties of goethite single crystal nanowires. *CrystEngComm* **2013,** *15*, 4905-4909.
10. Guo, H.; Barnard, A. S., Modeling the iron oxides and oxyhydroxides for the prediction of environmentally sensitive phase transformations. *Phys. Rev. B* **2011,** *83*, 1-18.
11. Alexandrov, V.; Rosso, K. M., Electron transport in pure and substituted iron oxyhydroxides by small-polaron migration. *J. Chem. Phys.* **2014,** *140*, 234701-1-8.
12. Fuente, S. A.; Belelli, P. G.; Castellani, N. J.; Avena, M., LDA +U and GGA +U studies of Al-rich and bulk goethite (a-FeOOH). *Mater. Chem. Phys.* **2013,** *137*, 1012-1020.
13. Pankhurst, Q. A.; Fernández Barquín, L.; Lord, J. S.; Amato, A.; Zimmermann, U., Intrinsic magnetic relaxation in goethite. *Phys. Rev. B* **2012,** *85*, 1-11.
14. Neumark, D. M.; Lykke, K. R.; Andersen, T.; Lineberger, W. C., Laser photodetachment measurement of the electron affinity of atomic oxygen. *Physical Review A* **1985,** *32*, (3), 1890-1892.
15. NIST, Atomic Spectra Database Ionization Energies Form. *http://physics.nist.gov/PhysRefData/ASD/ionEnergy.html*.